On the Efficiency of Different Higher Order Turbulence Models Simulating the Convective Boundary Layer.

J. E. Finger and H. Schmidt

DFVLR Institut für Physik der Atmosphäre, Oberpfaffenhofen

(Manuscript received 06.05.1986, in revised form 23.07.1986)

Abstract:

The output of a laboratory convection experiment is taken as a measure for one-dimensional numerical simulations with the aid of two different statistical turbulence models. These models – they are of second and third order of closure, respectively – are compared with each other. The importance of specific terms in the second moment equations with respect to typical features of the convective boundary layer is discussed. To assist this, balances of the heat flux equation are presented. It turns out that turbulent diffusion may not be neglected in the absence of mean advection. This transport process is indispensable for the representation of counter gradient heat fluxes.

Zusammenfassung: Zur Frage der Leistungsfähigkeit verschiedener Turbulenzmodelle höherer Ordnung bei der Simulation der konvektiven Grenzschicht

Die Ergebnisse eines Laborexperiments zur Untersuchung der konvektiven Grenzschicht dienen als Vergleich für eindimensionale Simulationen mit Hilfe zweier verschiedener statistischer Turbulenzmodelle. Diese Modelle, von denen das eine zweiter, das andere dritter Schließungsordnung ist, werden miteinander verglichen. Einzelne Terme in den Gleichungen für die zweiten Momente werden bezüglich ihrer Bedeutung für die Darstellung typischer Eigenschaften der konvektiven Grenzschicht diskutiert. Bilanzen der Gleichung für den Wärmefluß sind dabei von Nutzen. Es zeigt sich, daß bei verschwindender mittlerer Advektion die turbulente Diffusion nicht vernachlässigt werden darf. Ihre Berücksichtigung als Transportprozeß ist unabdingbar, um Wärmeflüsse gegen den Gradienten der mittleren Temperatur errechnen zu können.

Résumé: Sur la valeur de différents modèles de turbulence d'ordre supérieur pour simuler la couche limite convective

Les résultats d'une expérience de laboratoire sur la convection sont utilisés pour apprécier les simulations numériques à une dimension de deux modèles statistiques de turbulence. Ces modèles – dont la fermeture est, respectivement, du deuxième et du troisième ordre – sont comparés entre eux. On discute l'importance de termes spécifiques dans les équations des moments du second ordre à l'égard de traits caractéristiques de la couche limite convective. A cette fin, on présente les bilans de l'équation du flux de chaleur. Il apparaît qu'on ne peut négliger la diffusion turbulente en l'absence d'une advection moyenne. Ce processus de transport est indispensable pour représenter les flux de chaleur dans la direction opposée à celle du gradient.

1 Introduction

Our aim is to simulate the convective boundary layer (CBL) with the help of a 1-D numerical model. What has to be taken into account? One needs a turbulence model, which represents the averaged convective structures and therefore is called a statistical model. Turbulence energy is supplied internally by buoyancy throughout the whole layer. In the absence of mean flow (free convection) shear production as a second source of turbulence is excluded. Thus simple eddy viscosity concepts for the closure of the

0005-8173/86/04 0505–13 $ 03.00/0

governing equations obviously fail, since they are usually dependent on the deformation tensor, which vanishes in this case. More complex turbulence models, considering balance equations at least for the second moments, take into account all production mechanisms and are one way out of the dilemma presented.

In this paper two higher order closure models are presented, which differ considerably in the complexity of the model equations. The one (M1) is a third order closure model with prognostic equations for the second order moments and diagnostic equations for the third order ones. The other one (M2) is of second order with one prognostic equation for the turbulence energy and algebraic expressions for the other variances and covariances. This type of model corresponds to level 2 1/2 in the nomenclature of MELLOR and YAMADA (1982), which in the following is referred to as MY 82.

MELLOR and YAMADA (1974, MY 74) have compared the results of different second order models with the Wangara data. The agreement was quite good even for the simpler versions of the models, but no justification of turbulence quantities was possible, because the measurements only gave vertical profiles of the mean first moments. In a more recent paper (MY 82) they demonstrate that the results of their 2 1/2-level model fit the data of WILLIS and DEARDORFF (1974) quite well. This experimental investigation of the CBL reveals the main turbulent characteristics inside a tank of water, heated from below.

In the meantime DEARDORFF and WILLIS (1985, DW 85) repeated their experiment. Some former results, e.g. the profiles of vertical energy and of temperature variance, have been revised. We used the outpout of this experiment for testing our models. We try to answer the question of how the second order equations can reproduce typical processes like entrainment or counter gradient heat fluxes. The specific terms realizing these processes are identified.

2 Equations of the Models

With respect to the conditions in a water tank we are concerned with an incompressible fluid. Therefore the continuity equation takes on the divergence free form and density varies only due to temperature fluctuations:

$$\partial\rho = -\rho_0\beta\partial T \tag{1}$$

where $\rho_0 = 1000\ \mathrm{kg/m^3}$ and the volumetric expansion coefficient $\beta = 2.3\ 10^{-4}\ \mathrm{K^{-1}}$. Momentum and thermodynamic equations can be simplified due to the special conditions in the free convection case. The only external force acting upon the fluid, is buoyancy. For this reason Reynolds averages of the physical variables are formed in horizontal planes. The mean values of horizontal velocity components u and v vanish, as well as all horizontal gradients of mean values. Further on the continuity equation implies zero vertical mean velocity w. Thus the Boussinesq approximated momentum equation is truncated to a high degree: The buoyancy term is balanced by the vertical gradients of Reynolds stresses and pressure. The equation for the mean temperature T, if there are no external forces, and molecular diffusion is ignored, reduces to:

$$\frac{\partial T}{\partial t} = -\frac{\partial}{\partial z}\overline{w'T'} \tag{2}$$

2.1 The equations for the second moments

The prognostic equations for turbulent momentum and scalarfluxes at high Reynolds numbers for an incompressible fluid can be found in textbooks like RODI (1980). In the special case of free convection these equations read:

$$\frac{\partial}{\partial t}\overline{u_i' u_j'} = \underbrace{-\frac{\partial}{\partial z}\overline{u_i' u_j' w'} - \frac{1}{\rho_0}\frac{\partial \overline{u_j' p'}}{\partial z}\delta_{i3} - \frac{1}{\rho_0}\frac{\partial \overline{u_i' p'}}{\partial z}\delta_{j3}}_{D_{ij}} + \underbrace{\overline{\frac{p'}{\rho_0}\left(\frac{\partial u_i'}{\partial x_j} + \frac{\partial u_j'}{\partial x_i}\right)}}_{\Pi_{ij}}$$

$$\underbrace{+ g\beta\overline{u_j' T'}\,\delta_{i3} + g\beta\overline{u_i' T'}\delta_{j3}}_{PB_{ij}} \underbrace{- 2\nu\,\overline{\frac{\partial u_i'}{\partial x_\varrho}\frac{\partial u_j'}{\partial x_\varrho}}}_{\epsilon_{ij}} \tag{3}$$

$$\frac{\partial}{\partial t}\overline{u_i' T'} = \underbrace{-\overline{u_i' w'}\frac{\partial T}{\partial z}}_{PG_{iT}} \underbrace{- \frac{\partial}{\partial z}\overline{u_i' w' T'} - \frac{1}{\rho_0}\frac{\partial \overline{T' p'}}{\partial z}\delta_{i3}}_{D_{iT}} + \underbrace{\overline{\frac{p'}{\rho_0}\frac{\partial T'}{\partial x_i}}}_{\Pi_{iT}} + \underbrace{g\beta\overline{T'^2}\delta_{i3}}_{PB_{iT}} \underbrace{- (\nu+\kappa)\,\overline{\frac{\partial u_i'}{\partial x_\varrho}\frac{\partial T'}{\partial x_\varrho}}}_{\epsilon_{iT}} \tag{4}$$

$$\frac{\partial}{\partial t}\overline{T'^2} = \underbrace{-2\,\overline{w' T'}\frac{\partial T}{\partial z}}_{PG_{TT}} \underbrace{- \frac{\partial}{\partial z}\overline{w' T'^2}}_{D_{TT}} \underbrace{- 2\kappa\,\overline{\frac{\partial T'}{\partial x_\varrho}\frac{\partial T'}{\partial x_\varrho}}}_{\epsilon_{TT}} \tag{5}$$

While the production terms due to mean gradients (PG) and buoyancy (PB) are directly computable, three classes of terms are normally unknown in these equations:

- pressure-gradient terms Π,
- dissipation terms ϵ and
- diffusive terms D (including triple correlations)

They need to be either parameterized or – in the case of triple correlations – closed by the introduction of third order closure.

2.2 Common parameterizations

We study the problem of free convection and try to learn, how special terms of the second moment equations describe it. We are not interested in the effects which different parameterizations may have on the results. Therefore we make use of well tried model approximations for the unknown correlations.

Both, the momentum and the heat flux equation contain pressure-gradient terms, which act to redistribute turbulent kinetic energy and reduce heat fluxes and anisotropic stresses, respectively. Analysis of the Poisson-equation for pressure fluctuation leads to a splitting of the pressure-strain term into three components:

$$\overline{\frac{p'}{\rho_0}\left[\frac{\partial u_i'}{\partial x_j} + \frac{\partial u_j'}{\partial x_i}\right]} = \Pi_{ij,1} + \Pi_{ij,2} + \Pi_{ij,3} \tag{6}$$

Rotta's 'return-to-isotropy-term' $\Pi_{ij,1}$ is proportional to the anisotropy of the stress tensor:

$$\Pi_{ij,1} = -c_{Rm}\frac{\sqrt{E}}{\varrho}\left(\overline{u_i' u_j'} - \frac{2}{3}\delta_{ij}E\right) \tag{7}$$

ℓ is the characteristic length scale, $E = 1/2\overline{u_i'^2}$ the turbulent kinetic energy. $\Pi_{ij,2}$ is proportional to the anisotropy of shear-production and therefore can be omitted under the special condition of no shear. $\Pi_{ij,3}$ was proposed by ZEMAN and LUMLEY (1976) and is proportional to the anisotropy of buoyant-production:

$$\Pi_{ij,3} = -c_{Bm}\beta(g_i\overline{u_j'T'} + g_j\overline{u_i'T'} - \frac{2}{3}\delta_{ij}g_3\overline{w'T'}) \tag{8}$$

where the vector of gravitational acceleration $g_i = (0, 0, g)$ and c_{Bm} is the corresponding empirical constant. The pressure-temperature gradient correlation is handled analoguously:

$$\frac{\overline{p'\partial T'}}{\rho_0 \partial x_i} = \Pi_{iT,1} + \Pi_{iT,3} = c_{RT}\frac{\sqrt{E}}{\ell}\overline{u_i'T'} - c_{BT}\beta g_i\overline{T'^2} \tag{9}$$

To parameterize the various molecular dissipation terms Kolmogoroff's hypothesis is adopted, which leads, applying local isotropy for the small turbulent scales, to:

$$\epsilon_{ij} = \frac{2}{3}c_{\epsilon m}\frac{E^{3/2}}{\ell}\delta_{ij} \tag{10}$$

$$\epsilon_{TT} = 2\,c_{\epsilon T}\frac{E^{1/2}\overline{T'^2}}{\ell} \tag{11}$$

$$\epsilon_{iT} = 0 \tag{12}$$

Equations (10) to (12) are directly derivable from the theory for turbulence in the inertial subrange and $c_{\epsilon m}$ and $c_{\epsilon T}$ are the corresponding constants. To close the set of equations Blackadar's empirical formulation for the length scale is adopted:

$$\ell_B = kz \Big/ \left(1 + \frac{kz}{\ell_0}\right) \tag{13a}$$

$$\ell_0 = \alpha \int_0^{z_{top}} \sqrt{E}\, z\, dz \Big/ \int_0^{z_{top}} \sqrt{E}\, dz \tag{13b}$$

where k is the Karman constant (k = 0.35), z_{top} is the height of the water surface, ℓ_0 is the maximum mixing length and α an empirical constant. This formulation fails in stably stratified layers, where E converges to zero. A modification proposed by DEARDORFF (1980) is used in this situation. It involves the Brunt-Vaisalla frequency:

$$\ell_S = 0.76\sqrt{E}\left(g\beta\frac{\partial T}{\partial z}\right)^{-1/2} \tag{14}$$

The required length scale ℓ is then the minimum of these two formulations: $\ell = \min(\ell_B, \ell_s)$.

The constants in Rotta's term and in the expressions for dissipation have been adopted from MY 82. The buoyancy part of the pressure parameterization (c_{Bm} and c_{BT}) corresponds to ZEMAN and LUMLEY (1976), whereas α has been set due to own experiences with various kinds of boundary layers. Thus our set of constants reads:

pressure-terms:	$c_{Rm} = 0.512$,	$c_{RT} = 0.636$,	$c_{Bm} = 3/10$,	$c_{BT} = 1/3$
dissipation:	$c_{\epsilon m} = 0.169$,	$c_{\epsilon T} = 0.140$		
lengthscale:	$\alpha = 0.2$			

The difference in the numerical values between the MY 82- and our constants stems from our use of E for turbulent energy, while MY 82 take $q^2 = 2E$ for this quantity. Choosing the values of our constants we took into account this difference, because not the constants themselves, but the total parameterized expression must equal each other.

2.3 Assumptions concerning M1

Model version M1 solves the full balance equations for the second order moments. This requests a closure at the third order level by introducing equations for the triple correlations. The assumptions of ZEMAN and LUMLEY (1976) are adopted for these equations:

1. the local rate of change of the third-order moments is approximately zero
2. local isotropy of the third-order moments for molecular terms is assumed
3. the quasi-normal-approximation (QNA) is used for the fourth-order moments which appear.

The QNA relates the fourth-order moments to moments of first and second order. These assumptions lead to diagnostic equations for the triple correlations (listed in parameterized form in the appendix), containing terms representing production, dissipation, diffusion and buoyancy. In contrast to M1, all second order models involving diffusion terms in the second moment equations, replace the divergence of triple correlations by downgradient diffusion assumptions. This does not allow for buoyancy effects, which is the main difference between it and our third order closure.
The result of these assumptions is a set of prognostic equations for the first and second-order moments (Equations (18)), involved in the current problem, and diagnostic equations for all triple correlations, representing the turbulent diffusion of turbulence variables (Appendix).

2.4 Assumptions concerning M2

In contrast to M1 additional physical assumptions are made for M2 concerning the second order moment equations (Equations (19)). The main simplifying aspects are

- local equilibrium and
- isotropic forcing.

Following the scaling arguments in MY 74 all material derivatives as well as diffusive transport terms are neglected in the second moment equations for the anisotropic shear stresses, heat fluxes and temperature variance. The equations for these quantities thus become diagnostic and no closure for third order moments is required. The state of turbulence is assumed to be in static equilibrium, and anisotropy is determined solely by local effects. A complete balance equation is solved only for the turbulent kinetic energy. The diffusive term, containing the triple correlation, is approximated by a downgradient diffusion parameterization:

$$\frac{\partial}{\partial x_i}\left(\overline{u_i'\left(\frac{u_i'u_j'}{2}+\frac{p'}{\rho_0}\right)}\right)=\frac{\partial}{\partial z}\left(\frac{5}{3}\varrho c_{3m}E^{1/2}\frac{\partial E}{\partial z}\right) \tag{15}$$

The coefficient c_{3m} is given the value of 0.2 in accordance with the MY 82-set of constants. All time dependent processes and vertical transports by turbulent diffusion are therefore restricted to the equation for the turbulence energy, which still influences all other turbulent moments via parameterization.
The production terms due to gradients of the mean variables can be split in the following way:

$$\overline{u_i'u_\varrho'}\frac{\partial u_j}{\partial x_\varrho}=\left(A_{i\varrho}+\frac{2}{3}\delta_{i\varrho}E\right)\frac{\partial u_j}{\partial x_\varrho} \tag{16a}$$

$$\overline{u_i'u_j'}\frac{\partial T}{\partial x_j}=\left(A_{ij}+\frac{2}{3}\delta_{ij}E\right)\frac{\partial T}{\partial x_j} \tag{16b}$$

As SCHEMM and LIPPS (1976) have demonstrated by means of a scale analysis, the anisotropic forcing (containing the anisotropic stress tensor A_{ij} as a factor) is negligible in comparison to the isotropic one (multiplied by $2/3\delta_{ij}E$). The only gradient production term, which does not vanish due to the special conditions in the free convection case, is the one in the heat flux equation.

2.5 Parameterized equations for the second moments

The prescribed assumptions transform Equations (3) through (5) and result in the set of Equations (18) for M1 and (19) for M2; the symbols in the headline are used without subscripts to design the type of term listed below:

$$E = 0.5\,(\overline{u'^2} + \overline{v'^2} + \overline{w'^2}) = 0.5\,q^2 \tag{18.1}$$

PTD	PG	PB	D	π	ϵ	
$\frac{\partial}{\partial t}\overline{u'^2} =$			$-\frac{\partial}{\partial z}\overline{u'^2 w'} - c_{Rm}\frac{E^{1/2}}{\ell}(\overline{u'^2} - \frac{2}{3}E) + \frac{2}{3}c_{Bm}\,g\beta\overline{w'T'}$		$-\frac{2}{3}c_{\epsilon m}\frac{E^{3/2}}{\ell}$	(18.2)
$\frac{\partial}{\partial t}\overline{v'^2} =$			$-\frac{\partial}{\partial z}\overline{v'^2 w'} - c_{Rm}\frac{E^{1/2}}{\ell}(\overline{v'^2} - \frac{2}{3}E) + \frac{2}{3}c_{Bm}\,g\beta\overline{w'T'}$		$-\frac{2}{3}c_{\epsilon m}\frac{E^{3/2}}{\ell}$	(18.3)
$\frac{\partial}{\partial t}\overline{w'^2} =$		$+2g\beta\overline{w'T'}$	$-\frac{\partial}{\partial z}\overline{w'^3} - c_{Rm}\frac{E^{1/2}}{\ell}(\overline{w'^2} - \frac{2}{3}E) - \frac{4}{3}c_{Bm}\,g\beta\overline{w'T'}$		$-\frac{2}{3}c_{\epsilon m}\frac{E^{3/2}}{\ell}$	(18.4)
$\frac{\partial}{\partial t}\overline{w'T'} =$	$-\overline{w'^2}\frac{\partial T}{\partial z}$	$+g\beta\overline{T'^2}$	$-\frac{\partial}{\partial z}\overline{w'^2 T'} - c_{RT}\frac{E^{1/2}}{\ell}\overline{w'T'}$	$-c_{BT}\,g\beta\overline{T'^2}$		(18.5)
$\frac{\partial}{\partial t}\overline{T'^2} =$	$-2\overline{w'T'}\frac{\partial T}{\partial z}$		$-\frac{\partial}{\partial z}\overline{w'T'^2}$		$-2c_{\epsilon T}\frac{E^{1/2}}{\ell}\overline{T'^2}$	(18.6)
$\frac{\partial E}{\partial t} =$		$+g\beta\overline{w'T'}$	$+\frac{\partial}{\partial z}\left(\frac{5}{3}\ell c_{3m}E^{1/2}\frac{\partial E}{\partial z}\right)$		$-c_{\epsilon m}\frac{E^{3/2}}{\ell}$	(19.1)
$0 =$		$-\frac{2}{3}g\beta\overline{w'T'}$		$-c_{Rm}\frac{E^{1/2}}{\ell}(\overline{u'^2} - \frac{2}{3}E) + \frac{2}{3}c_{Bm}\,g\beta\overline{w'T'}$		(19.2)
$0 =$		$-\frac{2}{3}g\beta\overline{w'T'}$		$-c_{Rm}\frac{E^{1/2}}{\ell}(\overline{v'^2} - \frac{2}{3}E) + \frac{2}{3}c_{Bm}\,g\beta\overline{w'T'}$		(19.3)
$0 =$		$+\frac{4}{3}g\beta\overline{w'T'}$		$-c_{Rm}\frac{E^{1/2}}{\ell}(\overline{w'^2} - \frac{2}{3}E) - \frac{4}{3}c_{Bm}\,g\beta\overline{w'T'}$		(19.4)
$0 = -\frac{2}{3}E\frac{\partial T}{\partial z}$		$+g\beta\overline{T'^2}$		$-c_{RT}\frac{E^{1/2}}{\ell}\overline{w'T'} - c_{BT}\,g\beta\overline{T'^2}$		(19.5)
$0 = -2\overline{w'T'}\frac{\partial T}{\partial z}$					$-2c_{\epsilon T}\frac{\overline{T'^2}E^{1/2}}{\ell}$	(19.6)

2.6 Numerical scheme and boundary conditions

Model equations M1 and M2 are solved on the same 50 point staggered grid. Corresponding to the laboratory equipment, the water depth of 0.4 m results in a grid spacing of $\Delta z = 0.008$ m. The quantities $\overline{w'T'}$ and all triple correlations are positioned at $z = K\Delta z$, $K = 0, 1, \ldots, 51$, whereas all other variables are computed at points $z = (K - 1/2)\Delta z$, $K = 0, 1, \ldots, 51$. For time-integration the Adams-Bashforth scheme is used at a time step of $\Delta t = 0.05$ s.

The initial condition for the temperature profile is given by the experimental data of DW 85 (curve A in Figure 1). In M1 all double correlations are set to zero except at the lowest level, where values are set

according to the similarity theory (the solutions are not very sensitive to these values). For M2, only E has to be initialized; a linearly decreasing profile is used with a bottom value according to the formulation in M1, and zero at the top. The temperature gradient in the lowest level, needed for the solution of Equations (18.5, 18.6, 19.5 and 19.6), is approximated by $\partial T/\partial z = T_*/kz$. The temperature scale T_* is given by Equation (21). The vertical gradient of all triple correlations is set to zero at the bottom as are all double and triple correlations at the upper boundary. Corresponding to the heat flux imposed at the bottom of the tank and building up the CBL, an adequate value has to be set for $\overline{w'T'}$ at the lower boundary. As DW 85 point out, some uncertainty remains about the determination of surface heat flux $\overline{w'T'_s}$ under conditions of vanishingly small mean flow. In our numerical experiments we have used a boundary value of $\overline{w'T'_s} = 1.4\ 10^{-3}$ K m/s, determined by integration of the measured temperature profiles for times $t_1 = 191$ s and $t_2 = 599$ s in Figure 1:

$$\overline{w'T'_s} = \int_0^{z_{top}} (\partial T/\partial t)\, dz \tag{17}$$

As the temperature profile is not known below z = 0.07 m, the assumption has been made that both curves are constant in z below this level. The same value for the bottom heat flux results from using the empirical formula $\overline{w'T'_s} = (z_i/1.2)\, \partial T_m/\partial t$, given by DW 85. T_m is the mean temperature in the CBL for a given time.

3 Results

In the following, sets of the experimental and numerical results are shown in the same figures. The turbulent quantities are normalized by the convective velocity w_*, the temperature scale T_* and the height z_i of the mixed layer. By using this normalization the results are independent on time and comparable to measurements of CBLs in different geometries. w_* and T_* are defined as

$$w_* = (\beta g\, \overline{w'T'_S}\, z_i)^{1/3} \tag{20}$$

and the temperature scale

$$T_* = \frac{\overline{w'T'_S}}{w_*} \tag{21}$$

3.1 Temperature profile

Figure 1 presents the mean temperature profiles from the DW 85 experiment and from our simulations. The measured and simulated temperature profiles agree well. Small differences in the warming rate of the whole mixed layer probably are due to the uncertainty in the bottom heat flux in the experiment. We suspect that during the initial phase, a larger heat flux has been imposed because our mean temperatures are systematically lower than in the experiment by a constant amount. We ensured that simulated and experimental curves would nearly overlay each other if the heat supply were increased during the initial period of 191 seconds (0.0019 mK/s). The measurements show the build up of a mixed layer, capped by an inversion at height z_i. During the experiment the temperature level in the convective layer increases and the inversion extends towards the stable layer above. A measure for the growth of the CBL is the dimensionless vertical velocity of the inversion height $(\partial z_i/\partial t)/w_*$. Table 1 shows the results of different laboratory, atmospheric and numerical experiments. The stratification below z_i is slightly stable down to a height of about $0.5z_i$ or somewhat more. The lower portion of the mixed layer is not shown.

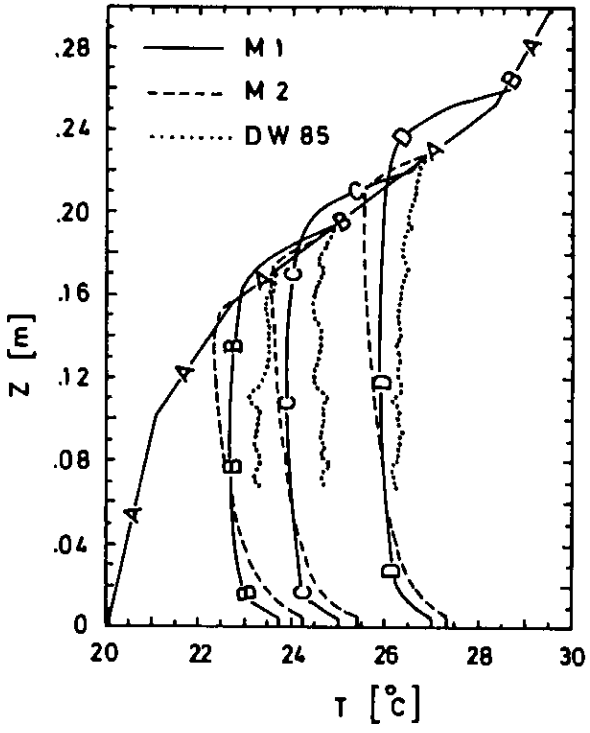

● **Figure 1** Temperature profile in a watertank, heated from below. Three different times have been chosen to plot the situation as observed in the DW 85 experiment and as simulated by the numerical models M1 and M2; A = Os, B = 191s, C = 328s, D = 599s.

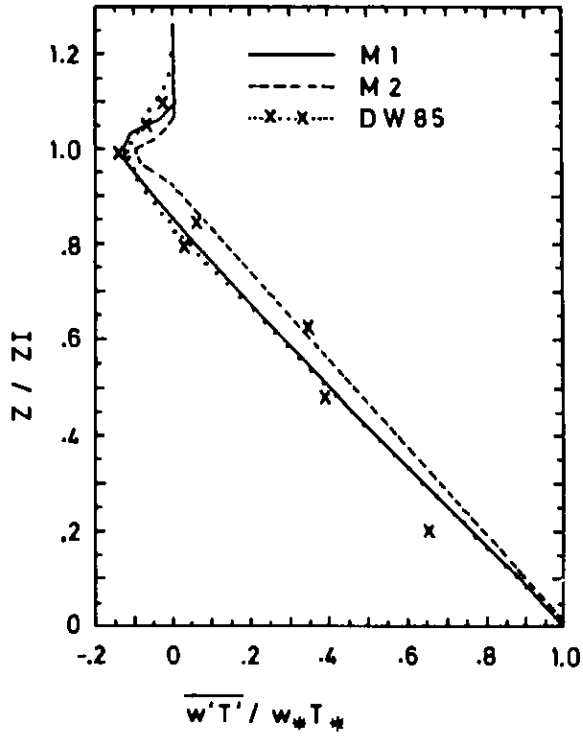

● **Figure 2** Heat flux profiles as measured in DM 85 and computed by M1 and M2 for time 599s, normalized by w_* and T_*.

■ **Table 1** Comparison of dimensionless vertical velocities of inversion height for different cases: A laboratory (DW 85), an atmospheric (KOOP 83, JOCHUM, 1985) and two numerical experiments (M1 and M2).

	DW 85	KOOP	M1	M2
$\frac{1}{w_*}\frac{\partial z_i}{\partial t}$	0.021	0.024	0.022	0.018

3.2 Heat flux

The profiles of the heat flux (Figure 2) exhibit a nearly linear decrease from the bottom to z_i. This is the typical behaviour of the heat flux in the steady state, when the build up phase of the CBL has ended. The constant gradient of $w'T'$ illustrates its well mixed character, insofar as each sublayer conducts the heat from below with the same resistance and absorbs the same amount of heat.

Following Equation (2) the temperature profile is mainly influenced by the divergence of the heat flux. Differentiation of this equation with respect to z shows that curvature in the $w'T'$-profile is only caused by time changes in the mean temperature gradient. $\partial T/\partial z$ varies in time due to the deepening of the CBL. Correspondingly the sharpest curvature of the heat flux is observed around z_i. The increase in inversion height also influences the mixed layer, but in its lower parts the temperature gradient becomes nearly independent of time and the deviation from linearity in the $w'T'$-profile is almost invisible.

A region of negative heat flux values is observed around z_i. It is caused by the mixing exchange between the convective and the stable layer. This physical process is called entrainment. Relatively cool fluid, driven by a large amount of vertical momentum, penetrates the inversion upward. Compensatory down-

draft of relatively warm fluid is set in motion. The result of this entrainment is a warming of the lower and a cooling of the upper interfacial region. The 'overshooting' of the temperature profile near z_i is a measure for the intensity of this process. The same holds for the extension and minimum amount of the heat flux. In the tank experiment, entrainment reaches from 0.8-1.2 z_i, the minimum value for $\overline{w'T'}$ is about $-10\,\%$ of $w'T'_s$.

In the case of M1 the agreement with the observed heat flux is perfect for all important features, while M2 underestimates the entrainment. This prediction could be improved by simply increasing the diffusion coefficient c_{3m} in the energy equation. Then a larger amount of E would be transported upwards near the inversion, where it triggers the heat flux minimum via the production term of Equation (19.5). Setting $c_{3m} = 1$ would be sufficient to obtain a result similar to M1. This gives a first hint that the turbulent diffusion is of decisive importance. It is confirmed in the Section 3.4.

3.3 Counter gradient flux

Since the observed experimental stratification (Figure 1) is stable at least above the lowest level of measurements, counter gradient heat fluxes prevail in the upper portion of the mixed layer (between approximately (0.5–0.8) z_i). Comparing the temperature profiles as simulated by the two numerical models, the most important difference is in the stability of the upper part of the CBL. M1 produces increasingly positive temperature gradients above approximately 0.5 z_i, while the heat flux changes its sign at about 0.85 z_i. Position and extension of the counter gradient flux region is therefore in very good accordance with the measurements. M2 on the other hand excludes the existence of a counter gradient heat flux on principle: Temperature gradient and $\overline{w'T'}$ are strictly coupled, which can be seen by reorganizing Equation (19.5):

$$\overline{w'T'} = \frac{-\frac{\ell}{c_{RT}}\frac{2}{3}E^{1/2}\frac{\partial T}{\partial z}}{1 + \frac{\ell^2}{c_{\epsilon T}c_{RT}E}(1-c_{RT})\,g\beta\frac{\partial T}{\partial z}} \tag{22}$$

The denominator also remains positive for negative temperature gradients, because for unstable stratification, E grows rapidly and keeps the second addend greater than minus one.

3.4 Heat flux balance

The comparison of the $\overline{w'T'}$-equations in M1 and M2 (Equations (18.5) and (19.5)) show a difference of three terms: Local rate of change, diffusion and production.

$$\frac{\partial}{\partial t}\overline{w'T'} = -\overline{w'^2}\frac{\partial T}{\partial z} + g\beta\overline{T'^2} - \frac{\partial}{\partial z}\overline{w'^2T'} - c_{RT}\frac{E^{1/2}}{\ell}\overline{w'T'} - c_{BT}\,g\beta\overline{T'^2} \tag{18.5}$$

$$0 = -\frac{2}{3}E\frac{\partial T}{\partial z} + g\beta\overline{T'^2} - c_{RT}\frac{E^{1/2}}{\ell}\overline{w'T'} - c_{BT}\,g\beta\overline{T'^2} \tag{19.5}$$

Figure 3 shows the relative weight of all terms in the complete heat flux Equation (18.5) as a function of time at a fixed height of 20 cm. From this plot one can get a hint of how good the assumptions are, which lead to Equation (19.5). As soon as the CBL reaches this position (after about 190 s) a heat flux is established, as reflected by the rapid evolution of gradient- and buoyant production. After the passage of the inversion, processes PG, PB, D and Π are of the same order of magnitude. The neglection of the diffusion term seems not to be justified by this simulation. On the other hand the local rate of change really plays the role of a small residuum and the assumption of quasi-stationarity will not cause a serious error. The replacement of the full production term by the isotropic assumption $\overline{w'^2}\partial T/\partial z = 2/3E\partial T/\partial z$ is expected

to be of minor importance. M1 predicts the vertical turbulence energy to be of the order of E. Thus M2 will underestimate the influence of this term.

If it is correct that the diffusion term in the heat flux Equation (18.5) is the decisive one for the simulation of counter gradient heat flux, its neglection should produce results very similar to those of M2. We have proved this statement by an additional numerical test: The turbulent diffusion in Equations (18.5) and (18.6) has been switched off by setting the triple correlations $\overline{w'^2T'}$ and $\overline{w'T'^2}$ equal to zero, whereas the time dependency remained unchanged. As major results the entrainment zone diminished and the temperature profile lost its stable portion above 0.5 z/z_i totally. The removal of turbulent diffusion in the equations for heatflux and temperature variance makes the counter gradient flux vanish. The result also confirms, that in this context the time derivative is relatively meaningless.

The heat flux budget at a fixed time is plotted in Figure 4. The statement about the importance of the diffusive transport is also verified by its vertical distribution. Additionally, an insight is gained into how turbulent diffusion supports positive heat fluxes in a stably stratified environment. It works as a sink in the lower part of the mixed layer, where the production terms are positive. Above the level where the lapse rate changes sign, turbulent diffusion becomes a source and balances the negative mean gradient production.

Corresponding to the Rotta parameterization, the pressure gradient term is proportional to the anisotropy of the $w'T'$-correlation, weighted by the amount of turbulent kinetic energy. A CBL is by its nature highly anisotropic and therefore the Π-term makes a large contribution to the budget in nearly all of the layer. Near the inversion the dominant process is the negative production due to the strong stable stratification, while buoyant production – reflecting the typical relative maximum of $\overline{T'^2}$ (Figure 6) –, pressure and diffusion terms counteract this effect.

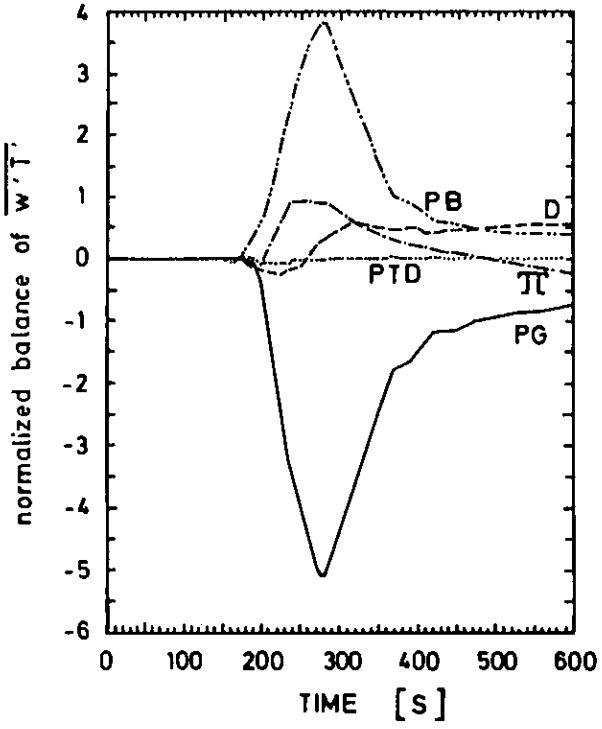

● **Figure 3** Time series of all terms in the heat flux Equation (18.5) at z=20 cm, normalized by $(w_*\overline{w'T'_s})/z_i$; $PG = -\overline{w'^2}(\partial T/\partial z)$, $PB = (1 - c_{BT})\, g\beta\overline{T'^2}$, $\Pi = -c_{RT}(E^{1/2}/\ell)\,\overline{w'T'}$, $D = -(\partial\overline{w'^2T'}/\partial z)$, $PTD = \partial\overline{w'T'}/\partial t$

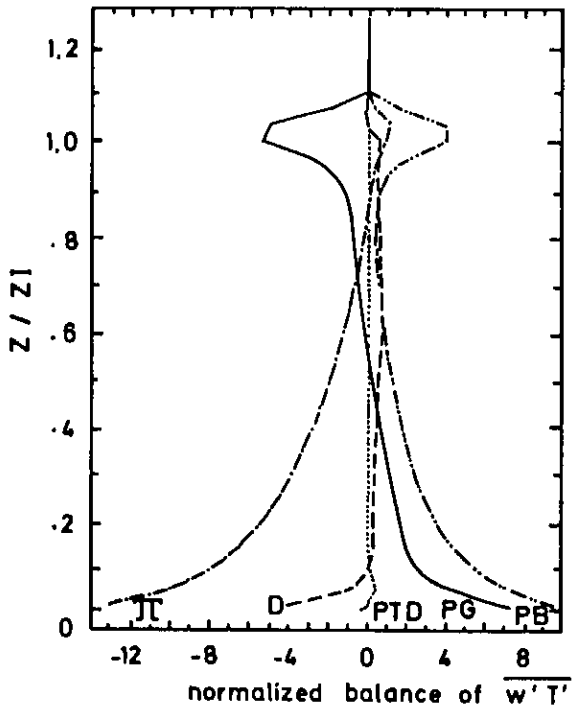

● **Figure 4** Budget of the heat flux equation at the fixed time 599s, normalization and symbols as in Figure 3.

3.5 Variances of w' and T'

The distribution of vertical energy is plotted in Figure 5. Both models show the typical CBL-maximum of w'^2 at a height of 0.3 z_i to 0.4 z_i, agreeing well with the data, although M1 underestimates and M2 overestimates this value. This effect can be eliminated in each model by 'fitting' the constant c_{Rm}, which controls redistribution between the different turbulence energy components. One other point should be noted: Near the inversion a higher intensity is observed in the experiment than in the numerical predictions. Especially the profile computed by M2 shows a very rapid decrease in the upper mixed layer. The vertical transport of this quantity is insufficient as pointed out in Section 3.2.

The most striking feature of the temperature variance profile (Figure 6) is the secondary maximum at z_i. As can be seen from Equations (18.6) and (19.6) it is produced by the heat flux minimum in combination with the stable stratification in this layer. For this reason the M1-peak is more distinct than that computed by M2. The latter seems to agree better with the experimental result in this region. Another difference is to be noticed at a height of 0.9 z_i: While in the case M2 the temperature variance vanishes, M1 predicts a normalized value of about 1.0 for T'^2. Again, the reason for this effect is the turbulent diffusion in M1 which transports the variance into this region, where the production term is zero or very small.

4 Conclusions

The most important conclusion which can be drawn from the comparison between M1 and M2 is that turbulent diffusion may not be neglected. The relevance of this statement is restricted to 1-D

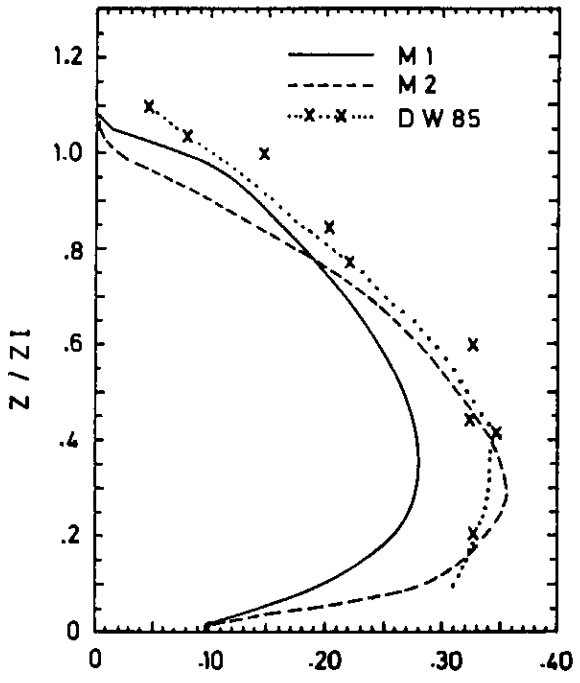

● **Figure 5** Vertical turbulent kinetic energy as measured in DW 85 and computed by M1 and M2 at time 599s, normalized by w_*

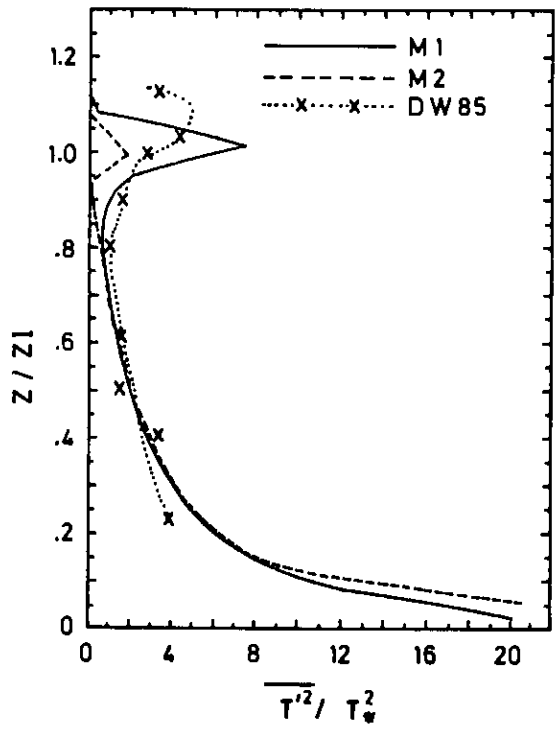

● **Figure 6** Variance of temperature fluctuation T' as measured in DW 85 and computed by M1 and M2 at time 599s, normalized by T_*

statistical simulations. We are aware, that the diffusion terms in our system represent physical processes, which cannot be described by these kinds of models. Neither the rising of warm bubbles nor any transport by mean vertical velocity can be resolved. Thus diffusion is the only transport at all in our equations and necessarily of high importance. M2 takes into account turbulent diffusion only in the energy equation. Although this is coupled with the equations of all other turbulent quantities, this formulation evidently is not sufficient to simulate processes like entrainment or counter gradient heat fluxes adequately. The assumptions that lead to model equations M1 and M2 are rough. In particular we think of the 1-dimensional approach to turbulence, which is in principal 3-D. Keeping this in mind, the agreement with the DW 85 experiment is surprisingly good. This is one justification for these simple models. Another is the very modest demand for computer resources. We have applied a large-eddy-simulation to the same experimental situation, using the full M2-model (which comprises diagnostic equations for all anisotropic shear stresses and heat fluxes) for representation of the subgrid-scale. The need for computer time for a $8 \times 8 \times 50$ grid exceeded the 1-D-simulation by a factor of 150. The temperature profiles do not look significantly different from the M1-result. If the prediction of mean profiles is the user's only interest, the M1 model can be recommended for problems of the free convection type.

APPENDIX

Third-Order Equations

Diagnostic equations for third-order moments for M1, depending on the parameterization of ZEMAN and LUMLEY (1976) and the formulation of CHEN and COTTON (1983):

$$\overline{T'^3} = -\frac{3}{1+3G1} c_{3T} \frac{\ell}{\sqrt{E}} \left(\overline{w'T'} \frac{\partial}{\partial z} \overline{T'^2} + c_{3K} \frac{\ell}{\sqrt{E}} B1 \frac{\partial T}{\partial z} \right) \tag{A01}$$

$$\overline{w'T'^2} = c_{3K} \frac{\ell}{\sqrt{E}} (B1 + g\beta \overline{T'^3}) \tag{A02}$$

$$\overline{w'^2T'} = c_{3F} \frac{\ell}{\sqrt{E}} \left(-2\overline{w'^2} \frac{\partial}{\partial z} \overline{w'T'} - \overline{w'T'} \frac{\ell}{\partial z} \overline{w'^2} + \frac{5}{3} g\beta \overline{w'T'^2} \right) \tag{A03}$$

$$\overline{w'^3} = c_{3K} \frac{\ell}{\sqrt{E}} \left(-3\overline{w'^2} \frac{\partial}{\partial z} \overline{w'^2} + \frac{13}{5} g\beta \overline{w'^2T'} \right) \tag{A04}$$

$$\overline{u'^2w'} = c_{3K} \frac{\ell}{\sqrt{E}} \left(-\overline{w'^2} \frac{\partial}{\partial z} \overline{u'^2} + \frac{1}{5} g\beta \overline{w'^2T'} \right) \tag{A05}$$

$$\overline{v'^2w'} = c_{3K} \frac{\ell}{\sqrt{E}} \left(-\overline{w'^2} \frac{\partial}{\partial z} \overline{v'^2} + \frac{1}{5} g\beta \overline{w'^2T'} \right) \tag{A06}$$

$$B1 = -\overline{w'^2} \frac{\partial}{\partial z} \overline{T'^2} - 2\overline{w'T'} \frac{\partial}{\partial z} \overline{w'T'} \tag{A07}$$

$$G1 = c_{G1} \frac{\ell^2}{E} g\beta \frac{\partial T}{\partial z} \tag{A08}$$

G1 was first introduced by CHEN and COTTON (1983) to include the dependence of triple correlations on thermal stability and to ensure that $\overline{T'^3}$, $\overline{w'T'^2}$ and $\overline{w'^2T'}$ are positive near the surface.

The constants used for the triple correlations are dependent on those for the second moments. After some albegra on the equations for ℓ and E as well as the different timescales of second and third-order moments τ and τ_3 ($\tau_3 = \tau/2.33$), we get:

$$c_{3T} = 3.52,\ c_{3K} = 1.08,\ c_{3F} = 1.01,\ c_{G1} = 3.80$$

As the QNA is utilized and OGURA (1962) showed that the use of this QNA in solving the equations may produce negative variances, ANDRÉ (1976) introduced the clipping approximation for third-order moments. This clipping approximation takes the damping effect of the fourth-order moments on the third-order ones into account and limits the magnitude of the triple correlations. The clipping approximation is imposed to insure that:

$$|\overline{a'b'c'}| \leq \min \begin{matrix} [\overline{a'^2}\,(\overline{b'^2}\ \ \overline{c'^2} + \overline{b'c'}^2)]^{1/2} \\ [\overline{b'^2}\,(\overline{a'^2}\ \ \overline{c'^2} + \overline{a'c'}^2)]^{1/2} \\ [\overline{c'^2}\,(\overline{a'^2}\ \ \overline{b'^2} + \overline{a'b'}^2)]^{1/2} \end{matrix}$$

where a, b, c stand for any of the models' turbulent fluctuating quantities. Numerical experiments with M1 show that in this application, the clipping approximation is only useful in computing $\overline{T'^3}$, while it is not necessary for the other triple correlations.

References

ANDRÉ, J.C., DE MOOR, G., LACARRERE, P. and DU VACHAT, R., 1976:
- Turbulence approximation for inhomogenous flows, Part I: The clipping approximation. J. Atmos. Sci. 33, 476–481
- Turbulence approximation for inhomogenous flows, Part II: The numerical simulation of a penetrative convection experiment. J. Atmos. Sci. 33, 482–491.

CHEN, C. and COTTON, W.R., 1983: Numerical experiments with a one-dimensional higher order turbulence model: Simulation of the Wangara Day 33. Boundary-Layer Meteor. 25, 375–404.

DEARDORFF, J.W. 1980: Stratocumulus-capped mixed layers derived from a three-dimensional model. Boundary-Layer Meteor. 18, 495–527

DEARDORFF, J.W. and WILLIS, G.E., 1985: Further results from a laboratory model of the convective planetary boundary layer. Boundary-Layer Meteor. 32, 205–236.

JOCHUM, A.M., 1985: The vertical structure of the convective boundary layer from motorglider-observations. OSTIV-proceedings XIX. congress, Rieti.

MELLOR, G.L. and YAMADA, T., 1974: A hierarchy of turbulence closure models for planetary boundary layers. J. Atmos. Sci. 31, 1791–1805.

MELLOR, G.L. and YAMADA, T., 1982: Development of a turbulence closure model for geophysical fluid problems. Rev. Geophys. Space Phys. 20.

OGURA, Y., 1962: Energy transfer in a normally distributed and isotropic turbulent velocity field in two dimensions. Phys. Fluids 5, 301–316.

RODI W., 1980: Turbulence models and their application in hydraulics. Delft, IAHR, 104 p.

SCHEMM, C.E. and LIPPS, F.B., 1976: Some results from a simplified three-dimensional numerical model of atmospheric turbulence. J. Atmos. Sci. 33, 1021–1041.

WILLIS, G.E. and DEARDORFF, J.W., 1974: A laboratory model of the unstable planetary boundary layer. J. Atmos. Sci. 31, 1297–1307.

ZEMAN, O. and LUMLEY, J.L., 1976: Modeling buoyancy driven mixed layers. J. Atmos. Sci. 33, 1974–1988.